

双光腔光机械系统的动力学相变和选择性能量交换

刘妮 张小芳 梁九卿

Dynamical phase transition and selective energy exchange in dual-cavity optomechanical systems

Liu Ni Zhang Xiao-Fang Liang Jiu-Qing

引用信息 Citation: *Acta Physica Sinica*, 70, 140301 (2021) DOI: 10.7498/aps.70.20210178

在线阅读 View online: <https://doi.org/10.7498/aps.70.20210178>

当期内容 View table of contents: <http://wulixb.iphy.ac.cn>

您可能感兴趣的其他文章

Articles you may be interested in

有限温度下腔光机械系统中 N 个二能级原子的相变和热力学性质

Phase transition and thermodynamic properties of N two-level atoms in an optomechanical cavity at finite temperature

物理学报. 2019, 68(19): 193701 <https://doi.org/10.7498/aps.68.20190347>

一种广义三模腔光机械系统的相干完美吸收与透射

Coherent perfect absorption and transmission of a generalized three-mode cavity optomechanical system

物理学报. 2017, 66(10): 107101 <https://doi.org/10.7498/aps.66.107101>

窗口声阻抗对锆相变动力学的影响

Phase transformation kinetics of zirconium under ramp wave loading with different windows

物理学报. 2018, 67(7): 070204 <https://doi.org/10.7498/aps.67.20172198>

高压下纳米晶ZnS晶粒和晶界性质及相变机理

Grain and grain boundary characteristics and phase transition of ZnS nanocrystallines under pressure

物理学报. 2020, 69(14): 147202 <https://doi.org/10.7498/aps.69.20200240>

利用连续激光抽运-太赫兹探测技术研究单晶和多晶二氧化钒纳米薄膜的相变

Study of phase transition of single crystal and polycrystalline vanadium dioxide nanofilms by using continuous laser pump-terahertz probe technique

物理学报. 2020, 69(20): 204205 <https://doi.org/10.7498/aps.69.20201188>

基于腔光力学系统的全光三极管的压缩特性

Squeezed property of optical transistor based on cavity optomechanical system

物理学报. 2019, 68(17): 174202 <https://doi.org/10.7498/aps.68.20190078>

双光腔光机械系统的动力学相变 和选择性能量交换*

刘妮[†] 张小芳 梁九卿

(山西大学理论物理研究所, 量子光学与光量子器件国家重点实验室, 太原 030006)

(2021 年 1 月 25 日收到; 2021 年 3 月 2 日收到修改稿)

本文探究了单腔和双腔光机械装置的动力学相变和选择性能量交换. 发现系统会经历类似于 Dicke-Hepp-Lieb 超辐射型的动力学相变, 且两光场间的正交动量耦合出现一个新的动力学临界点. 两光场间的正交动量耦合等价于单(双)模光机械系统的外场驱动. 通过耦合参数的调控, 系统可以实现任意两模间的选择性能量交换, 且临界耦合点与选择性能量交换对应. 模压缩是能量转换的标志, 且任何两模的正交压缩由特定玻色模间的能量交换决定.

关键词: 双光腔光机械系统, 相变, 选择性能量交换, 模压缩

PACS: 03.65.-w, 42.50.Pq, 05.30.Rt, 73.43.Nq

DOI: 10.7498/aps.70.20210178

1 引言

光腔和纳米机械振子之间的电磁耦合导致了宏观量子系统的新的量子力学行为^[1], 而且实验上已经在单光子水平上实现了这种新奇的量子系统^[1-4], 同时理论上已研究了单模光机械腔的强耦合特性, 且发现: 当光场和机械振子的耦合远大于腔场衰减和机械振荡频率时, 这些混合系统中的量子效应出现. 通过在光腔内放置 Kerr 介质, 量子非线性也可被引入到系统中^[5]. 实验已经证明, 通过将两个光模耦合到一个机械振子上来显著增强量子非线性^[6,7], 该增强的量子非线性在光子数的量子非破坏测量方面具有潜在的应用. 根据腔内光场与机械振子之间通过辐射压形成的非线性反馈耦合机制, 机械振子一方面可以有效冷却并表现出宏观量子效应; 另一方面可以诱导可观测的少光子非线性光学效应. 相反, 也可以改变机械振子的特

征实现对光场的调节和控制. 光机械系统在量子信息处理中也具有应用前景. Kerr 型非线性可以作为全光开关的基础, 并应用于光子或声子比特的量子相位门的设计^[8]. 机械模可作为量子信息处理中的长程记忆, 它可存储光脉冲中包含的全部量子信息^[9]. 光学和机械自由度之间的相互作用产生固态、光学比特和原子比特之间的量子交叉. 总之, 光机械腔系统^[10-12]在量子测量研究中取得了阶段性的成果, 而且展示出广泛的应用前景. 此外, 光机械腔系统在量子调控、量子模拟、高精度测量, 以及微电子工业等方面也展现出重要的应用价值, 特别是与微纳技术和冷原子技术结合后, 该系统正发展成为研究量子测量与量子操控的理想平台. 一系列新颖的基于光机械腔系统的量子测量方案展示出该系统在量子测量、量子操控等方面的潜在应用. 近年来, 两模系统在理论上得到了广泛研究, 且由两光学模和机械振子模构成的三模系统最近也被用于研究多粒子量子关联^[13]. 可见, 研究双

* 国家自然科学基金(批准号: 11772177, 12047571)和山西省高等学校科技创新项目(批准号: 2019L0069)资助的课题.

[†] 通信作者. E-mail: 317446484@qq.com

光腔光机械系统^[10–12]的基态特性具有重要的科学价值.

基于光机械系统的广泛应用, 我们得到: 两光学模耦合到一个机械模的线性化哈密顿量, 该系统的动力学相变与 Dicke 模型的动力学相变类似^[14–17]. 另外, 两个超强耦合的谐振子系统能展示类似于 Dicke 超辐射相变的特性. 我们主要计算了不同光机械系统正常模的表达式, 且通过调控耦合参数, 系统可以经历类似于 Dicke–Hepp–Lieb 型超辐射类型的动力学相变. 同时证实了任何两模之间的选择性能量交换的可能性, 最后还研究了量子临界点附近的模压缩与选择性能量交换的对应性. 这些结果对量子测量和量子计算有一定的参考价值.

2 动力学相变模型

2.1 光机械腔

光机械腔系统如图 1 所示. 图 1 光机械腔系统的哈密顿量表示如下:

$$H = H_0 + H_{\text{int}}, \quad (1)$$

其中自由能哈密顿量 H_0 和相互作用哈密顿量 H_{int} 分别为:

$$H_0 = \hbar\omega_0 a^\dagger a + \hbar\omega_m b^\dagger b, \quad (2)$$

$$H_{\text{int}} = -\hbar g a^\dagger a (b + b^\dagger) + i\hbar (\mu a^\dagger e^{-i\omega_L t} - \mu^* a e^{i\omega_L t}). \quad (3)$$

相互作用哈密顿量 (3) 式来自于腔模频率的空间依赖性, 当机械位移足够小时线性阶成为相互作用中惟一重要的项.

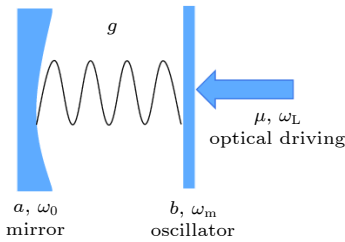


图 1 光机械腔系统, 由频率为 ω_0 的光学模 (用运算符 a 表示), 频率为 ω_m 的机械模 (用运算符 b 表示) 和频率为 ω_L (振幅为 μ) 的驱动场组成, 光腔与机械振子之间的耦合系数为 g

Fig. 1. An optomechanical cavity consisting of the optical mode (the frequency ω_0) denoted by a , the mechanical mode b (the frequency ω_m) and an pair of optical drivings (the frequency ω_L and the amplitude μ) with the coupling strength g .

以泵浦场驱动频率 ω_L 做旋转, 系统的哈密顿量表示为

$$H = \hbar\omega_s a^\dagger a + \hbar\omega_m b^\dagger b - \hbar g a^\dagger a (b + b^\dagger) + i\hbar (\mu a^\dagger - \mu^* a), \quad (4)$$

其中 $\omega_s = \omega_0 - \omega_L$ 为腔膜与驱动场之间的失谐.

根据海森伯–朗之万方程, 基于哈密顿 (4) 式可得系统相关算符的运动方程为:

$$\dot{a}(t) = -i\omega_s a(t) + i g a(t) [b(t) + b^\dagger(t)] + \mu - \frac{\gamma_c}{2} a(t) + \sqrt{\gamma_c} a_{\text{in}}(t), \quad (5)$$

$$\dot{b}(t) = -i\omega_m b(t) - i g a^\dagger(t) a(t) - \gamma_m b(t) + \sqrt{\gamma_m} \xi(t), \quad (6)$$

其中 $a_{\text{in}}(t)$ 是光学模的输入噪声算子, 其特征值是光子衰减率 γ_c ; $\xi(t)$ 是由机械模的布朗运动引起的噪声算子.

我们将每个算符写成稳态平均值和零平均涨落值, 即 $a \rightarrow \alpha + a$, $b \rightarrow \beta + b$. 对海森伯–朗之万方程 (5) 式和 (6) 式求平均值得到其演化方程:

$$\langle \dot{a}(t) \rangle = -i\omega_s \langle a(t) \rangle + i g \langle a(t) \rangle \langle b(t) + b^\dagger(t) \rangle + \mu - \frac{\gamma_c}{2} \langle a(t) \rangle, \quad (7)$$

$$\langle \dot{b}(t) \rangle = -i\omega_m \langle b(t) \rangle + i g \langle a^\dagger(t) a(t) \rangle - \gamma_m \langle b(t) \rangle. \quad (8)$$

各算符的稳态平均值和哈密顿量分别为:

$$\alpha = \frac{\mu}{i\omega_s + \gamma_c/2 - i g (\beta^\dagger + \beta)}, \quad (9)$$

$$\beta = \frac{i g \alpha^\dagger \alpha}{i\omega_m + \gamma_m}, \quad (10)$$

$$H = \hbar(\omega_s - 2g\beta) a^\dagger a + \hbar\omega_m b^\dagger b - \hbar g \alpha (a^\dagger + a) (b^\dagger + b) + \hbar(\omega_s \alpha - 2g\alpha\beta) (a^\dagger + a) + \hbar(\omega_m \beta - g\alpha^2) (b^\dagger + b) - \hbar g (a^\dagger a b^\dagger + a^\dagger a b) + \hbar\omega_m \beta^2 + \hbar\omega_s \alpha^2 - 2\hbar g \alpha^2 \beta. \quad (11)$$

为了对角化, 忽略常数项和齐次项, 仅保留双线性项, 即令 $\omega_s \alpha - 2g\alpha\beta = 0$ 和 $\omega_m \beta - g\alpha^2 = 0$, 整理 (11) 式得到系统的有效哈密顿量:

$$H_{\text{eff}} = \hbar\omega a^\dagger a + \hbar\omega_m b^\dagger b - \hbar\eta (a^\dagger + a) (b^\dagger + b), \quad (12)$$

其中, $\omega = \omega_s - 2g\beta$ 和 $\eta = g\alpha$ 决定了波动的稳态值. 依据坐标、动量和算符的关系

$$\begin{cases} x = \frac{1}{\sqrt{2\omega}} (a^\dagger + a), & p_x = i\sqrt{\frac{\omega}{2}} (a^\dagger - a), \\ y = \frac{1}{\sqrt{2\omega_m}} (b^\dagger + b), & p_y = i\sqrt{\frac{\omega_m}{2}} (b^\dagger - b), \end{cases} \quad (13)$$

将 (13) 式代入有效哈密顿量 (12) 式中, 整理化简可得:

$$H_{\text{eff}} = \frac{1}{2}(\omega^2 x^2 + \omega_m^2 y^2 - 4\eta\sqrt{\omega\omega_m}xy + p_x^2 + p_y^2). \quad (14)$$

通过如下方式对系统坐标进行旋转, 消除 xy 相互作用项,

$$\begin{cases} x = q_1 \cos \phi + q_2 \sin \phi, \\ y = -q_1 \sin \phi + q_2 \cos \phi, & \tan 2\phi = \frac{4\eta\sqrt{\omega\omega_m}}{\omega^2 - \omega_m^2}, \\ p_x = p_1, & p_y = p_2, \end{cases} \quad (15)$$

则 (14) 式化简为无耦合振子

$$H_{\text{eff}} = \frac{1}{2}(\varepsilon_1^2 q_1^2 + \varepsilon_2^2 q_2^2 + p_1^2 + p_2^2), \quad (16)$$

其中, ε_1 和 ε_2 的值为:

$$\varepsilon_1^2 = \frac{1}{2}[\omega^2 + \omega_m^2 + \sqrt{(\omega^2 - \omega_m^2)^2 + 16\eta^2\omega\omega_m}], \quad (17)$$

$$\varepsilon_2^2 = \frac{1}{2}[\omega^2 + \omega_m^2 - \sqrt{(\omega^2 - \omega_m^2)^2 + 16\eta^2\omega\omega_m}], \quad (18)$$

通过引入以下两种 q 玻色模来重新量化哈密顿量 (16) 式, 即

$$\begin{cases} q_1 = \sqrt{\frac{1}{2\varepsilon_1}} (c_1^\dagger + c), & p_1 = i\sqrt{\frac{\varepsilon_1}{2}} (c_1^\dagger - c), \\ q_2 = \sqrt{\frac{1}{2\varepsilon_2}} (c_2^\dagger + c_2), & p_2 = i\sqrt{\frac{\varepsilon_2}{2}} (c_2^\dagger - c_2). \end{cases} \quad (19)$$

则重新量化的哈密顿量为

$$H_{\text{eff}} = \varepsilon_1 c_1^\dagger c_1 + \varepsilon_2 c_2^\dagger c_2 + \frac{1}{2}(\varepsilon_1 + \varepsilon_2). \quad (20)$$

根据激发能 (17) 式和 (18) 式, 结合 (20) 式可知: 当 $\varepsilon_2^2 < 0$ 时, 对应于机械振子模 $c_2^\dagger c_2$ 的特征值 ε_2 可以为虚数, 此时满足 $\eta > \sqrt{\omega\omega_m}/2$, 如图 2 红线所示. 这意味着系统经历了不同的行为过程, 这取决于 $\varepsilon_2^2 < 0$ 时的不稳定相或 $\varepsilon_2^2 > 0$ 时的稳定相. 动力学相变的稳定相对应于正常相到超辐射量子相变的正常相, 而动力学相变的不稳定相 (在动力学临界点 $\eta = \sqrt{\omega\omega_m}/2$ 的右侧) 对应于正常相到超辐射量子相变的超辐射相. 值得注意的是, 尽管有效哈密顿量 (12) 式显示出类似于 Dicke-Hepp-Lieb 相变的变化, 但由于仅存在两模, 而量子相变发生在多模系统中, 所以该系统本质上并不是严格

的量子相变. $c_1^\dagger c_1$ 玻色模的特征值 ε_1 (黑线) 始终是真实的, 而 $c_2^\dagger c_2$ 玻色模的特征值 ε_2 (红线) 通过调节参数可以变成虚数. 当 $\eta > \sqrt{\omega\omega_m}/2$ 时, 特征值 ε_2 变为虚数, 对应超辐射相.

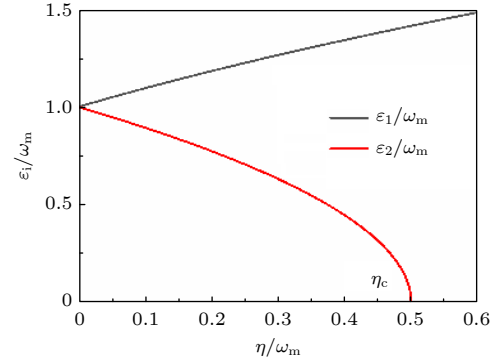


图 2 在给定条件 $\omega = \omega_m$ 下, 激发能量 ε_i/ω_m 随耦合参数 η/ω_m 的变化

Fig. 2. Variation of the excitation energy ε_i/ω_m with respect to the coupling parameter η/ω_m in the case of $\omega = \omega_m$.

2.2 双光腔光机械系统

2.2.1 双光腔间无耦合

双光腔光机械系统如图 3 所示. 图 3 系统对应的哈密顿量为:

$$H_0 = \hbar \sum_{i=1}^2 \omega_i a_i^\dagger a_i + \hbar \omega_m b^\dagger b, \quad (21)$$

$$\begin{aligned} H_{\text{int}} = & -\hbar \sum_{i=1}^2 g_i a_i^\dagger a_i (b + b^\dagger) \\ & + i\hbar \sum_{i=1}^2 (\mu_i a_i^\dagger e^{-i\omega_L t} - \mu_i^* a_i e^{i\omega_L t}). \end{aligned} \quad (22)$$

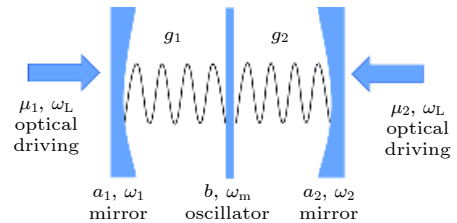


图 3 双光腔光机械系统, 由频率分别为 ω_1 和 ω_2 的光学模 (用运算符 a_1 和 a_2 表示), 频率为 ω_m 的机械模 (用运算符 b 表示) 和频率为 ω_L (振幅为 μ_i) 的两束对打的驱动场组成, 两模光腔与机械振子之间的耦合系数分别为 g_1 和 g_2 .
Fig. 3. A double-optical cavity optomechanical system consisting of two optical mode (the frequencies ω_1 and ω_2) denoted by a_1 and a_2 , the mechanical mode b (the frequency ω_m) and an pair of optical drivings (the frequency ω_L and the amplitude μ_i) with the coupling strength g_1 and g_2 .

相对驱动场频率 ω_L 作旋转后, 系统的哈密顿量写为

$$H = \omega_m b^\dagger b + \hbar \sum_{i=1}^2 [\omega_{si} a_i^\dagger a_i - g_i a_i^\dagger (b + b^\dagger) + i(\mu_i a_i^\dagger - \mu_i^* a_i)], \quad (23)$$

其中, ω_{si} 为腔膜与驱动场之间的失谐, $\omega_{si} = \omega_i - \omega_L$ ($i = 1, 2$).

根据海森伯-朗之万方程可得系统相关算符的运动方程为:

$$\dot{a}_i(t) = -i\omega_{si} a_i(t) + ig_i a_i(t) [b(t) + b^\dagger(t)] + \mu_i - \frac{\gamma_{ci}}{2} a_i(t) + \sqrt{\gamma_{ci}} a_{in_i}(t), \quad (24)$$

$$\dot{b}(t) = -i\omega_m b(t) + ig_1 a_1^\dagger(t) a_1(t) + ig_2 a_2^\dagger(t) a_2(t) - \gamma_m b(t) + \sqrt{\gamma_m} \xi(t), \quad (25)$$

其中, $a_{in_i}(t)$ 是光学模的输入噪声算子, 其特征值是光子衰减率 γ_{ci} ; $\xi(t)$ 是由机械模的布朗运动引起的噪声算子. 并将每个算符写成稳态平均值和零平均涨落值, 即 $a_i \rightarrow \alpha_i + a_i$, $b \rightarrow \beta + b$, 对海森伯-朗之万方程 (24) 式和 (25) 式求平均值, 得到其演化方程:

$$\langle \dot{a}_i(t) \rangle = -i\omega_{si} \langle a_i(t) \rangle + ig_i \langle a_i(t) \rangle \langle b(t) \rangle + \langle b^\dagger(t) \rangle + \mu_i - \frac{\gamma_{ci}}{2} \langle a_i(t) \rangle, \quad (26)$$

$$\langle \dot{b}(t) \rangle = -i\omega_m \langle b(t) \rangle + ig_1 \langle a_1^\dagger(t) a_1(t) \rangle + ig_2 \langle a_2^\dagger(t) a_2(t) \rangle - \gamma_m \langle b(t) \rangle. \quad (27)$$

各算符的稳态平均值和哈密顿量分别为:

$$\langle a_i(t) \rangle = \alpha_i = \frac{\mu_i}{i\omega_{si} + \gamma_{ci}/2 - ig_i(\beta^\dagger + \beta)}, \quad (28)$$

$$\langle b(t) \rangle = \beta = \frac{ig_1 \alpha_1^\dagger \alpha_1 + ig_2 \alpha_2^\dagger \alpha_2}{i\omega_m + \gamma_m}, \quad (29)$$

$$H = \hbar\omega_m b^\dagger b + \hbar\omega_m \beta^2 + \hbar \sum_{i=1}^2 [\omega_{si} \alpha_i^2 - 2\beta g_i \alpha_i^2] + \hbar \sum_{i=1}^2 [(\omega_{si} - 2g_i \beta) a_i^\dagger a_i - g_i \alpha_i (a_i^\dagger + a_i) \times (b^\dagger + b) + (\omega_{si} \alpha_i - 2\beta g_i \alpha_i) (a_i^\dagger + a_i) + (\omega_m \beta - g_i \alpha_i^2) (b^\dagger + b) - g_i a_i^\dagger a_i (b^\dagger + b)]. \quad (30)$$

仅保留双线性项, 即令: $\omega_{si} \alpha_i - 2\beta g_i \alpha_i = 0$, $\omega_m \beta - g_i \alpha_i^2 = 0$, 整理 (30) 式得到系统的有效哈密顿量:

$$H = \hbar\omega_m b^\dagger b + \hbar \sum_{i=1}^2 [\Omega_i a_i^\dagger a_i - \hbar G_i (a_i^\dagger + a_i) (b^\dagger + b)], \quad (31)$$

其中, $\Omega_i = \omega_{si} - 2g_i \beta$, $G_i = g_i \alpha_i$ ($i = 1, 2$), 决定了波动的稳态值.

基于如下的坐标、动量与算符的关系将哈密顿量 (31) 式进行重新量化,

$$\begin{cases} x = \frac{1}{\sqrt{2\Omega_1}} (a_1^\dagger + a_1), \\ p_x = i\sqrt{\frac{\Omega_1}{2}} (a_1^\dagger - a_1), \\ y = \frac{1}{\sqrt{2\Omega_2}} (a_2^\dagger + a_2), \\ p_y = i\sqrt{\frac{\Omega_2}{2}} (a_2^\dagger - a_2), \\ z = \frac{1}{\sqrt{2\omega_m}} (b^\dagger + b), \\ p_z = i\sqrt{\frac{\omega_m}{2}} (b^\dagger - b), \end{cases} \quad (32)$$

经整理可得:

$$H_{\text{eff}} = \frac{1}{2} [\Omega_1^2 x^2 + \Omega_2^2 y^2 + \omega_m^2 z^2 - 4G_1 \sqrt{\Omega_1 \omega_m} xz - 4G_2 \sqrt{\Omega_2 \omega_m} yz + p_x^2 + p_y^2 + p_z^2]. \quad (33)$$

与 2.1 节中对角化方式类似, 通过如下方式对系统坐标进行旋转, 消除 xz 和 yz 相互作用项:

$$\begin{cases} x = q_1 (1 + \cos \phi_1) + q_3 \sin \phi_1, \\ y = q_2 (1 + \cos \phi_2) + q_3 \sin \phi_2, \\ z = -q_1 \sin \phi_1 - q_2 \sin \phi_2 + q_3 (\cos \phi_1 + \cos \phi_2), \\ p_x = p_1, \\ \tan 2\phi_1 = \frac{4G_1 \sqrt{\Omega_1 \omega_m}}{\Omega_1^2 - \omega_m^2}, \\ \tan 2\phi_2 = -\frac{4G_2 \sqrt{\Omega_2 \omega_m}}{\Omega_2^2 - \omega_m^2}, \\ p_y = p_2, \\ p_z = p_3. \end{cases} \quad (34)$$

则 (33) 式化简为

$$H_{\text{eff}} = \frac{1}{2} \sum_{i=1}^3 \left(\frac{\varepsilon_i^2 q_i^2}{2} + p_i^2 \right), \quad (35)$$

其中 ε_i 为

$$\varepsilon_1^2 = \frac{1}{2} \left[(2\Omega_1^2 + \Omega_2^2 + \omega_m^2) + \sqrt{(\Omega_1^2 - \omega_m^2)^2 + 16G_1^2\Omega_1\omega_m} - \sqrt{(\Omega_2^2 - \Omega_1^2)^2} \right], \quad (36)$$

$$\varepsilon_2^2 = \frac{1}{2} \left[(\Omega_1^2 + 2\Omega_2^2 + \omega_m^2) + \sqrt{(\Omega_2^2 - \omega_m^2)^2 + 16G_2^2\omega_m\Omega_2} + \sqrt{(\Omega_2^2 - \Omega_1^2)^2} \right], \quad (37)$$

$$\varepsilon_3^2 = \frac{1}{2} \left[(\Omega_1^2 + \Omega_2^2 + 2\omega_m^2) - \sqrt{(\Omega_1^2 - \omega_m^2)^2 + 16G_1^2\Omega_1\omega_m} - \sqrt{(\Omega_2^2 - \omega_m^2)^2 + 16G_2^2\omega_m\Omega_2} \right]. \quad (38)$$

我们现在通过引入以下三种玻色模来重新量化哈密顿量 (35) 式:

$$\begin{cases} q_1 = \sqrt{\frac{1}{2\varepsilon_1}} (c_1^\dagger + c_1), & p_1 = i\sqrt{\frac{\varepsilon_1}{2}} (c_1^\dagger - c_1), \\ q_2 = \sqrt{\frac{1}{2\varepsilon_2}} (c_2^\dagger + c_2), & p_2 = i\sqrt{\frac{\varepsilon_2}{2}} (c_2^\dagger - c_2), \\ q_3 = \sqrt{\frac{1}{2\varepsilon_3}} (c_3^\dagger + c_3), & p_3 = i\sqrt{\frac{\varepsilon_3}{2}} (c_3^\dagger - c_3). \end{cases} \quad (39)$$

此变换下的哈密顿量为

$$H_{\text{eff}} = \sum_{i=1}^3 \left(\varepsilon_i c_i^\dagger c_i + \frac{\varepsilon_i}{2} \right). \quad (40)$$

共振情形 ($\Omega_1 = \Omega_2 = \omega_m$) 下, 能量泛函 (36) 式—(38) 式退化为

$$\begin{aligned} \frac{\varepsilon_1}{\omega_m} &= \sqrt{2 \left(1 + \frac{G_1}{\omega_m} \right)}, & \frac{\varepsilon_2}{\omega_m} &= \sqrt{2 \left(1 + \frac{G_2}{\omega_m} \right)}, \\ \frac{\varepsilon_3}{\omega_m} &= \sqrt{2 \left(1 - \frac{G_1}{\omega_m} - \frac{G_2}{\omega_m} \right)}. \end{aligned} \quad (41)$$

基于 (41) 式, 图 4 给出了无耦合的双光腔光机械系统的激发能谱, 其中 ε_1/ω_m (黑线) 和 ε_2/ω_m (红线) 是光学分支, ε_3/ω_m (蓝线) 是声子分支, 从图可以观测到能量的选择性转移. 从图 4(a) 可以看到光学模 c_1 (黑线) 和声子模 c_3 (蓝线) 之间的能量交换, 而光学模 c_2 (红线) 没有变化; 从图 4(b) 可以看到光学模 c_2 和声子模 c_3 之间的能量交换, 而光学模 c_1 没有变化. ε_3/ω_m (蓝线) 展示了在某个临界耦合参数 $G_{1c}(G_{2c})$ 处的动态相变. 当 $G_1 \leq G_{1c}$ ($G_2 \leq G_{2c}$) 时, 激发能量 ε_3/ω_m 为实数, 对应正常相; 当 $G_1 > G_{1c}$ ($G_2 > G_{2c}$) 时, 激发能量 ε_3/ω_m 变为虚数, 对应超辐射相. 图中相边界点满足条件

$$G_1 + G_2 = \omega_m. \quad (42)$$

2.2.2 双光腔间有耦合

双光腔间有耦合的机械系统如图 5 所示. 图 5

的哈密顿量为:

$$H_0 = \hbar \sum_{i=1}^2 \omega_i a_i^\dagger a_i + \hbar \omega_m b^\dagger b, \quad (43)$$

$$H_{\text{int}} = -\hbar \left[\sum_{i=1}^2 g_i a_i^\dagger a_i - J (a_1 a_2^\dagger + a_2 a_1^\dagger) \right] (b^\dagger + b). \quad (44)$$

相互作用哈密顿量 (44) 式是由腔频的空间依赖性

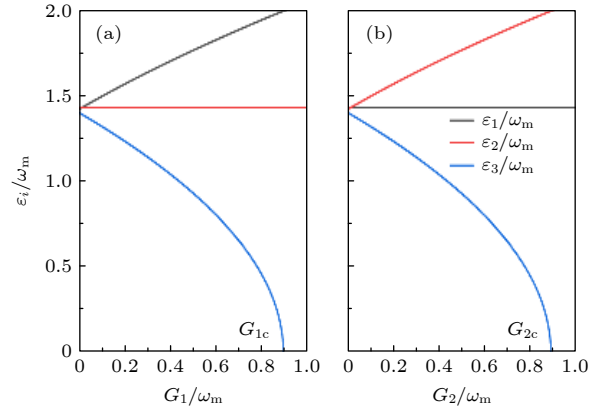


图 4 激发能量 ε_i/ω_m 随耦合参数 (a) G_1/ω_m 和 (b) G_2/ω_m 的变化, 给定的参数是 $\Omega_1 = \Omega_2 = \omega_m$

Fig. 4. Variation of the excitation energy ε_i/ω_m with respect to the coupling parameters (a) G_1/ω_m and (b) G_2/ω_m . The given parameters are $\Omega_1 = \Omega_2 = \omega_m$.

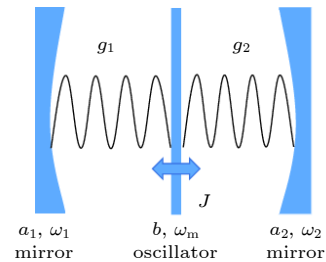


图 5 双光腔光机械系统, 由频率分别为 ω_1 和 ω_2 的光学模 (用运算符 a_1 和 a_2 表示) 和频率为 ω_m 的机械模 (用运算符 b 表示) 组成, 两模光腔与机械振子之间的耦合系数分别为 g_1 和 g_2 , 两腔间与机械振子的耦合系数为 J

Fig. 5. A double-optical cavity optomechanical system consisting of two optical mode (the frequencies ω_1 and ω_2) denoted by a_1 and a_2 and the mechanical mode b with the coupling strength g_1 , g_2 and J .

引起的, 其中 J 表示两光学模与机械振子之间的耦合, 它对应于相干的克尔类型相互作用, 将量子非线性引入了系统^[7]. 当机械位移足够小时, 线性阶

成为相互作用中惟一重要的项. 实验上通常在腔体中间放入薄膜来实现^[6].

系统相关算符的运动方程为:

$$\dot{a}_1(t) = -i\omega_1 a_1(t) + ig_1 a_1(t) [b(t) + b^\dagger(t)] - iJ a_2(t) [b(t) + b^\dagger(t)] - \frac{\gamma_{c_1}}{2} a_1(t) + \sqrt{\gamma_{c_1}} a_{in_1}(t), \quad (45)$$

$$\dot{a}_2(t) = -i\omega_2 a_2(t) + ig_2 a_2(t) [b(t) + b^\dagger(t)] - iJ a_1(t) [b(t) + b^\dagger(t)] - \frac{\gamma_{c_2}}{2} a_2(t) + \sqrt{\gamma_{c_2}} a_{in_2}(t), \quad (46)$$

$$\dot{b}(t) = -i\omega_m b(t) + ig_1 a_1^\dagger(t) a_1(t) + ig_2 a_2^\dagger(t) a_2(t) - iJ [a_1(t) a_2^\dagger(t) + a_2(t) a_1^\dagger(t)] - \gamma_m b(t) + \sqrt{\gamma_m} \xi(t). \quad (47)$$

接下来将每个算符写成稳态平均值和零平均涨落值, 即 $a_i \rightarrow \alpha_i + a_i$, $b \rightarrow \beta + b$. 再对海森伯-朗之万方程 (45) 式—(47) 式求平均值, 得其演化方程:

$$\langle \dot{a}_1(t) \rangle = -i\omega_1 \langle a_1(t) \rangle + ig_1 \langle a_1(t) \rangle \langle b(t) + b^\dagger(t) \rangle - iJ \langle a_2(t) \rangle \langle b(t) + b^\dagger(t) \rangle - \frac{\gamma_{c_1}}{2} \langle a_1(t) \rangle, \quad (48)$$

$$\langle \dot{a}_2(t) \rangle = -i\omega_2 \langle a_2(t) \rangle + ig_2 \langle a_2(t) \rangle \langle b(t) + b^\dagger(t) \rangle - iJ \langle a_1(t) \rangle \langle b(t) + b^\dagger(t) \rangle - \frac{\gamma_{c_2}}{2} \langle a_2(t) \rangle, \quad (49)$$

$$\langle \dot{b}(t) \rangle = -i\omega_m \langle b(t) \rangle + ig_1 \langle a_1^\dagger(t) a_1(t) \rangle + ig_2 \langle a_2^\dagger(t) a_2(t) \rangle - iJ \langle a_1(t) a_2^\dagger(t) + a_2(t) a_1^\dagger(t) \rangle - \gamma_m \langle b(t) \rangle. \quad (50)$$

各算符的稳态平均值和哈密顿量分别为:

$$\alpha_1 = \frac{iJ\alpha_2(\beta + \beta^\dagger)}{[ig_1(\beta + \beta^\dagger) - (i\omega_1 + \frac{\gamma_{c_1}}{2})]}, \quad (51)$$

$$\alpha_2 = \frac{iJ\alpha_1(\beta + \beta^\dagger)}{[ig_2(\beta + \beta^\dagger) - (i\omega_2 + \frac{\gamma_{c_2}}{2})]}, \quad (52)$$

$$\beta = \frac{i \sum_{i=1}^2 g_i \alpha_i^\dagger \alpha_i - iJ(\alpha_1 \alpha_2^\dagger + \alpha_2 \alpha_1^\dagger)}{(i\omega_m + \gamma_m)}, \quad (53)$$

$$\begin{aligned} H = & \hbar \sum_{i=1}^2 (\omega_i - 2g_i \beta) a_i^\dagger a_i + \hbar \omega_m b^\dagger b - \hbar \sum_{i=1}^2 \left[(g_1 \alpha_1 - J\alpha_2) (a_1^\dagger + a_1) + (g_2 \alpha_2 - J\alpha_1) (a_2^\dagger + a_2) \right] (b^\dagger + b) \\ & + \hbar (\omega_1 \alpha_1 + 2\beta J\alpha_2 - 2\beta g_1 \alpha_1) (a_1^\dagger + a_1) + \hbar (\omega_2 \alpha_2 + 2\beta J\alpha_1 - 2\beta g_2 \alpha_2) (a_2^\dagger + a_2) \\ & + \hbar 2\beta J (a_1 a_2^\dagger + a_2 a_1^\dagger) + \hbar \left(\omega_m \beta + 2J\alpha_1 \alpha_2 - \sum_{i=1}^2 g_i \alpha_i^2 \right) (b^\dagger + b) - \hbar \sum_{i=1}^2 g_i a_i^\dagger a_i (b^\dagger + b) \\ & + \hbar J (a_2 a_1^\dagger + a_1 a_2^\dagger) (b^\dagger + b) + \hbar \omega_m \beta^2 + \hbar \sum_{i=1}^2 \omega_i \alpha_i^2 + \hbar 4\beta J\alpha_1 \alpha_2 - \hbar \sum_{i=1}^2 2\beta g_i \alpha_i^2. \end{aligned} \quad (54)$$

保留双线性项后, 整理得到系统的有效哈密顿量:

$$H_{\text{eff}} = \hbar \sum_{i=1}^2 \Omega_i a_i^\dagger a_i + \hbar \omega_m b^\dagger b - \hbar \sum_{i=1}^2 J_i (a_i^\dagger + a_i) (b^\dagger + b) + \hbar \delta (a_1 a_2^\dagger + a_2 a_1^\dagger), \quad (55)$$

其中, $\Omega_i = \omega_i - 2\beta g_i$, $J_1 = g_1 \alpha_1 - J\alpha_2$, $J_2 = g_2 \alpha_2 - J\alpha_1$, $\delta = 2J\beta$, $\omega_1 \alpha_1 + 2\beta J\alpha_2 - 2\beta g_1 \alpha_1 = 0$, $\omega_2 \alpha_2 + 2\beta J\alpha_1 - 2\beta g_2 \alpha_2 = 0$, $\omega_m \beta + 2J\alpha_1 \alpha_2 - \sum_{i=1}^2 g_i \alpha_i^2 = 0$. 这些条件决定了波动的稳态值.

$$\begin{cases} x = \frac{1}{\sqrt{2\Omega_1}} (a_1^\dagger + a_1), & p_x = i\sqrt{\frac{\Omega_1}{2}} (a_1^\dagger - a_1), & y = \frac{1}{\sqrt{2\Omega_2}} (a_2^\dagger + a_2), & p_y = i\sqrt{\frac{\Omega_2}{2}} (a_2^\dagger - a_2), \\ z = \frac{1}{\sqrt{2\omega_m}} (b^\dagger + b), & p_z = i\sqrt{\frac{\omega_m}{2}} (b^\dagger - b). \end{cases} \quad (56)$$

将坐标动量关系 (56) 式代入 (55) 式将哈密顿量进行对角化:

$$H_{\text{eff}} = \frac{1}{2} \left[\Omega_1^2 x^2 + \Omega_2^2 y^2 + \omega_m^2 z^2 - 4J_1 \sqrt{\Omega_1 \omega_m} xz - 4J_2 \sqrt{\Omega_2 \omega_m} yz + 2\delta \sqrt{\Omega_1 \Omega_2} xy + 2\delta \frac{p_x p_y}{\sqrt{\Omega_1 \Omega_2}} + p_x^2 + p_y^2 + p_z^2 \right]. \quad (57)$$

与 2.1 节, 2.2 节中对角化方式类似, 可以通过如下方式对系统坐标进行旋转来消除相互作用项 $xy, xz, yz, p_x p_y$:

$$\begin{cases} x = q_1 (\cos \phi_1 + \cos \phi_2) + q_2 \sin \phi_1 + q_3 \sin \phi_2, & \tan 2\phi_1 = \frac{2\delta \sqrt{\Omega_1 \Omega_2}}{\Omega_2^2 - \Omega_1^2}, \\ y = -q_1 \sin \phi_1 + q_2 (\cos \phi_1 + \cos \phi_3) + q_3 \sin \phi_3, & \tan 2\phi_2 = \frac{4J_1 \sqrt{\Omega_1 \omega_m}}{\Omega_1^2 - \omega_m^2}, \\ z = -q_1 \sin \phi_2 - q_2 \sin \phi_3 + q_3 (\cos \phi_2 + \cos \phi_3), & \tan 2\phi_3 = -\frac{4J_2 \sqrt{\Omega_2 \omega_m}}{\Omega_2^2 - \omega_m^2}, \\ p_x = p_1, p_y = p_2, p_z = p_3. \end{cases} \quad (58)$$

再通过如下动量关系进行旋转来消除相互作用项 $p_x p_y$:

$$p_x = p_1 \cos \phi_4 + p_2 \sin \phi_4, \quad p_y = -p_1 \sin \phi_4 + p_2 \cos \phi_4, \quad p_z = p_3. \quad (59)$$

当角度满足 $\cos \phi_4 = 0$ 时, 则哈密顿量 (55) 式化简为

$$H_{\text{eff}} = \frac{1}{2} \left(\frac{\varepsilon_I^2 q_I^2}{2} + \frac{\varepsilon_{\text{II}}^2 q_{\text{II}}^2}{2} + \frac{\varepsilon_{\text{III}}^2 q_{\text{III}}^2}{2} + \varepsilon_{p_I} p_I^2 + \varepsilon_{p_{\text{II}}} p_{\text{II}}^2 + p_{\text{III}}^2 \right), \quad (60)$$

其中 $\varepsilon_I, \varepsilon_{\text{II}}, \varepsilon_{\text{III}}, \varepsilon_{p_I}, \varepsilon_{p_{\text{II}}}$ 为:

$$\varepsilon_I^2 = \frac{1}{2} \left[(2\Omega_1^2 + \Omega_2^2 + \omega_m^2) + \sqrt{(\Omega_1^2 - \omega_m^2)^2 + 16J_1^2 \Omega_1 \omega_m} - \sqrt{(\Omega_2^2 - \Omega_1^2)^2 + 4\delta^2 \Omega_1 \Omega_2} \right], \quad (61)$$

$$\varepsilon_{\text{II}}^2 = \frac{1}{2} \left[(\Omega_1^2 + 2\Omega_2^2 + \omega_m^2) + \sqrt{(\Omega_2^2 - \Omega_1^2)^2 + 4\lambda^2 \Omega_1 \Omega_2} + \sqrt{(\Omega_2^2 - \omega_m^2)^2 + 16J_2^2 \omega_m \Omega_2} \right], \quad (62)$$

$$\varepsilon_{\text{III}}^2 = \frac{1}{2} \left[(\Omega_1^2 + 2\Omega_2^2 + \omega_m^2) - \sqrt{(\Omega_2^2 - \Omega_1^2)^2 + 16J_1^2 \omega_m \Omega_1} - \sqrt{(\Omega_2^2 - \omega_m^2)^2 + 16J_2^2 \omega_m \Omega_2} \right], \quad (63)$$

$$\varepsilon_{p_I} = 1 - \frac{\delta}{\sqrt{\Omega_1 \Omega_2}}, \quad \varepsilon_{p_{\text{II}}} = 1 + \frac{\delta}{\sqrt{\Omega_1 \Omega_2}}, \quad (64)$$

我们现在通过引入三种新的玻色模 (65) 式来重新量化哈密顿量 (60) 式:

$$\begin{cases} q_I = \sqrt{\frac{\varepsilon_{p_I}}{2\varepsilon_I}} (c_1^\dagger + c_1), & p_I = i\sqrt{\frac{\varepsilon_I}{2\varepsilon_{p_I}}} (c_1^\dagger - c_1), \\ q_{\text{II}} = \sqrt{\frac{\varepsilon_{p_{\text{II}}}}{2\varepsilon_{\text{II}}}} (c_2^\dagger + c_2), & p_{\text{II}} = i\sqrt{\frac{\varepsilon_{\text{II}}}{2\varepsilon_{p_{\text{II}}}}} (c_2^\dagger - c_2), \\ q_{\text{III}} = \sqrt{\frac{1}{2\varepsilon_{\text{III}}}} (c_3^\dagger + c_3), & p_{\text{III}} = i\sqrt{\frac{\varepsilon_{\text{III}}}{2}} (c_3^\dagger - c_3). \end{cases} \quad (65)$$

则哈密顿量 (60) 式整理为

$$H_{\text{eff}} = \varepsilon_{I'} c_1^\dagger c_1 + \varepsilon_{\text{II}'} c_2^\dagger c_2 + \varepsilon_{\text{III}'} c_3^\dagger c_3 + \frac{1}{2} [\varepsilon_{I'} + \varepsilon_{\text{II}'} + \varepsilon_{\text{III}'}], \quad (66)$$

其中, $\varepsilon_{I'} = \varepsilon_I \sqrt{\varepsilon_{p_I}}, \varepsilon_{\text{II}'} = \varepsilon_{\text{II}} \sqrt{\varepsilon_{p_{\text{II}}}}, \varepsilon_{\text{III}'} = \varepsilon_{\text{III}}, \varepsilon_{p_I} = 1 - \frac{\delta}{\sqrt{\Omega_1 \Omega_2}}, \varepsilon_{p_{\text{II}}} = 1 + \frac{\delta}{\sqrt{\Omega_1 \Omega_2}}.$

从本征值 (61) 式—(63) 式得出: 当 $\varepsilon_I^2 \varepsilon_{p_I} < 0$ 时, 对应于光学玻色模 $c_1^\dagger c_1$ 的特征值 $\varepsilon_{I'}$ 可以为虚数, 此时 $\delta > \sqrt{\Omega_1 \Omega_2}$, 如图 6(a) 黑线所示. 这意味着系统所经历的过程取决于 $\varepsilon_I^2 \varepsilon_{p_I} < 0$ 时的不稳定相或是 $\varepsilon_I^2 \varepsilon_{p_I} > 0$ 时的稳定相, 动力学相变的稳定相 ($\delta \leq \delta_c$) 对应于超辐射量子相变的正常相, 而动力学相变的不稳定相 ($\delta > \delta_c$) 对应于量子相变的超辐射相. 如同 2.1 节部分, 尽管有效哈密顿量 (55) 式展示出类似于 Dicke-Hepp-Lieb 跃迁的相

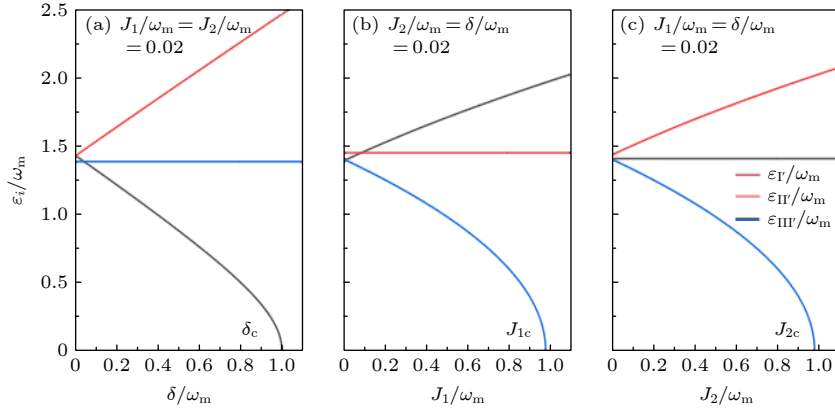

 图 6 激发能量 ε_i/ω_m 随耦合参数 (a) δ/ω_m , (b) J_1/ω_m 和 (c) J_2/ω_m 的变化, 给定的参数是 $\Omega_1 = \Omega_2 = \omega_m$

Fig. 6. Variation of the excitation energy ε_i/ω_m with respect to the coupling parameters (a) δ/ω_m , (b) J_1/ω_m and (c) J_2/ω_m . The given parameters are $\Omega_1 = \Omega_2 = \omega_m$.

变, 但只有三种模式存在, 故本质上仍不是严格的量子相变. 对应于光学玻色模 $c_2^\dagger c_2$ 的特征值 $\varepsilon_{II'}$ 始终是真实的, 如图 6 红线. 从图 6(b) 和图 6(c) 可以看出: 随耦合参数 J_1/ω_m (J_2/ω_m) 变化, 声子模 $c_3^\dagger c_3$ 的特征值 $\varepsilon_{III'}$ 在 $J_1 > J_{1c}$ ($J_2 > J_{2c}$) 变为虚数, 是声子分支 $\varepsilon_{III'}$ 的动态相变. 本文中不会详细讨论相变, 而且上述模型仅在稳定阶段有效. 图 6 展示

了光学分支 $\varepsilon_{I'}$, $\varepsilon_{II'}$ 和声子分支 $\varepsilon_{III'}$ 能量的选择性转移. 图 6(a) 显示两光学分支 $\varepsilon_{I'}$, $\varepsilon_{II'}$ 之间的能量转移, 而声子模的能量 $\varepsilon_{III'}$ 不改变. 临界耦合 $\delta_c = \sqrt{\Omega_1 \Omega_2}$ 显示动力学相变, 是两种光学模式的动量方程间耦合的结果. 从 (64) 式看出: 在某些参数下使 $\varepsilon_{p1} < 0$ 和 $\varepsilon_1^2 < 0$ 时, 特征值 $\varepsilon_{I'}$ 可取负值, 代表系统不稳定, 耦合参数 δ 满足

$$\delta_{us} = \frac{1}{2} \sqrt{\frac{\left(2\Omega_1^2 + \Omega_2^2 + \omega_m^2 + \sqrt{(\Omega_1^2 - \omega_m^2)^2 + 16J_1^2 \Omega_1 \omega_m}\right)^2 - (\Omega_2^2 - \Omega_1^2)^2}{\Omega_1 \Omega_2}}. \quad (67)$$

当没有其他模式的动量耦合时, δ_{us} 就是通常的动力学临界点 G_{1c} (G_{2c}), 如图 4 所示. 对于图 6(b) 给出光学模 $c_1^\dagger c_1$ 和声子模 $c_3^\dagger c_3$ 之间的能量交换, 在临界耦合 J_{1c} 处发生动力学相变, 临界耦合 J_{1c} 满足:

$$J_{1c} = \frac{1}{4} \sqrt{\frac{\left(\Omega_1^2 + \Omega_2^2 + 2\omega_m^2 - \sqrt{(\Omega_2^2 - \omega_m^2)^2 + 16J_2^2 \Omega_2 \omega_m}\right)^2 - (\Omega_1^2 - \omega_m^2)^2}{\Omega_1 \omega_m}}. \quad (68)$$

可见, 声子激发谱中的动力学相变表明在动力学临界点发生从机械模到光学模的完全能量转换 (蓝线-红线). 类似地图 6(c) 给出光学模 $c_2^\dagger c_2$ 和声子模 $c_3^\dagger c_3$ 之间的清晰能量转换.

3 模压缩

本节研究了多种玻色模的压缩特性. 如果玻色模的位置或动量正交不确定性小于其相干状态下的不确定性, 则称其被压缩 [18]. 相干态是满足 $(\Delta\alpha)^2(\Delta p_\alpha)^2 = 1/4$ [$\alpha = x, y, \dots$] 的最小不确定态, 且不确定性在两个正交之间平均分配. 如果 $(\Delta\alpha)^2 <$

$1/2$ 或 $(\Delta p_\alpha)^2 < 1/2$, 则玻色场被压缩 [18–20]. 原模式的两个正交方差被定义为 $(\Delta\alpha)^2 = \langle \alpha^2 \rangle - \langle \alpha \rangle^2$ 和 $(\Delta p_\alpha)^2 = \langle p_\alpha^2 \rangle - \langle p_\alpha \rangle^2$. 我们利用波戈留波夫变换 ($\alpha_k = u_k a_k - v_k b_k^\dagger$, $\beta_k = u_k b_k - v_k a_k^\dagger$, 且 $u_k^2 - v_k^2 = 1$) 给出原始玻色模 $[a, b, \dots]$ 和变换的玻色子模式 $[c_1, c_2, \dots]$ 之间的关系.

3.1 光机械腔

本节研究了两种玻色模的压缩特性. 原始玻色子模 $[a, b]$ 和重新量化的玻色模 $[c_1, c_2]$ 之间的关系利用波戈留波夫变换给出:

$$a^\dagger = \frac{1}{2} \left\{ \frac{\cos \phi}{\sqrt{\omega \varepsilon_1}} \left[(\omega + \varepsilon_1) c_1^\dagger + (\omega - \varepsilon_1) c_1 \right] + \frac{\sin \phi}{\sqrt{\omega \varepsilon_2}} \left[(\omega + \varepsilon_2) c_2^\dagger + (\omega - \varepsilon_2) c_2 \right] \right\}, \quad (69)$$

$$b^\dagger = \frac{1}{2} \left\{ \frac{-\sin \phi}{\sqrt{\omega_m \varepsilon_1}} \left[(\omega_m + \varepsilon_1) c_1^\dagger + (\omega_m - \varepsilon_1) c_1 \right] + \frac{\cos \phi}{\sqrt{\omega_m \varepsilon_2}} \left[(\omega_m + \varepsilon_2) c_2^\dagger + (\omega_m - \varepsilon_2) c_2 \right] \right\}. \quad (70)$$

基于 (69), (70) 式, 给出各变量的方差:

$$\begin{cases} (\Delta x)^2 = \frac{\cos^2 \phi}{2\varepsilon_1} + \frac{\sin^2 \phi}{2\varepsilon_2}, \\ (\Delta p_x)^2 = \cos^2 \phi \frac{\varepsilon_1}{2} + \sin^2 \phi \frac{\varepsilon_2}{2}, \\ (\Delta y)^2 = \frac{\sin^2 \phi}{2\varepsilon_1} + \frac{\cos^2 \phi}{2\varepsilon_2}, \\ (\Delta p_y)^2 = \sin^2 \phi \frac{\varepsilon_1}{2} + \cos^2 \phi \frac{\varepsilon_2}{2}. \end{cases} \quad (71)$$

基于 (69) 式, 图 7 给出了压缩方差 $(\Delta x)^2 \omega_m$ 和 $(\Delta y)^2 \omega_m$ (实线)、 $(\Delta p_x)^2 / \omega_m$ 和 $(\Delta p_y)^2 / \omega_m$ (虚线) 随耦合参数 η / ω_m 的变化, 注意由于 $\omega = \omega_m$, 所以 $(\Delta x)^2 \omega_m$ 和 $(\Delta y)^2 \omega_m$ 重合, $(\Delta p_x)^2 / \omega_m$ 和 $(\Delta p_y)^2 / \omega_m$

重合. 该图与图 2 激发谱随耦合参数的变化对应. 动量方差没有被压缩, 在接近临界耦合 η_c 时, 更加不被压缩而分离, 如图实线; 反之, 坐标方差被压缩, 而且接近临界耦合 η_c 时, 压缩更明显. 在动力学临界点处 (如图点线), 位置方差显示最大压缩, 可见, 压缩是能量转换的标志.

3.2 双光腔光机械系统

3.2.1 双光腔间无耦合

本节研究了光腔间无耦合的双模光机械腔的压缩特性. 原始玻色模 $[a_1, a_2, b]$ 和重新量化的玻色模 $[c_1, c_2, c_3]$ 之间的关系利用波戈留波夫变换给出:

$$a_1^\dagger = \frac{1}{2} \left\{ \frac{\cos \phi_1}{\sqrt{\Omega_1 \varepsilon_1}} \left[c_1^\dagger (\Omega_1 + \varepsilon_1) + c_1 (\Omega_1 - \varepsilon_1) \right] + \frac{\sin \phi_1}{\sqrt{\Omega_1 \varepsilon_3}} \left[c_3^\dagger (\Omega_2 + \varepsilon_3) + c_3 (\Omega_2 - \varepsilon_3) \right] \right\}, \quad (72)$$

$$a_2^\dagger = \frac{1}{2} \left\{ \frac{\cos \phi_2}{\sqrt{\Omega_2 \varepsilon_2}} \left[c_2^\dagger (\Omega_2 + \varepsilon_2) + c_2 (\Omega_2 - \varepsilon_2) \right] + \frac{\sin \phi_2}{\sqrt{\Omega_2 \varepsilon_3}} \left[c_3^\dagger (\Omega_2 + \varepsilon_3) + c_3 (\Omega_2 - \varepsilon_3) \right] \right\}, \quad (73)$$

$$\begin{aligned} b^\dagger = \frac{1}{2} \left\{ \frac{-\sin \phi_1}{\sqrt{\omega_m \varepsilon_1}} \left[c_1^\dagger (\omega_m + \varepsilon_1) + c_1 (\sqrt{\varepsilon_{p_1}} - \varepsilon_1) \right] - \frac{\sin \phi_2}{\sqrt{\omega_m \varepsilon_2}} \left[c_2^\dagger (\omega_m + \varepsilon_2) + c_2 (\omega_m - \varepsilon_2) \right] \right. \\ \left. + \frac{\cos \phi_1 + \cos \phi_2}{\sqrt{\omega_m \varepsilon_3}} \left[c_3^\dagger (\omega_m + \varepsilon_3) + c_3 (\omega_m - \varepsilon_3) \right] \right\}. \end{aligned} \quad (74)$$

基于 (72) 式—(74) 式, 很容易给出各变量的方差:

$$\begin{cases} (\Delta x)^2 = \frac{\cos^2 \phi_1}{2\varepsilon_1} + \frac{\sin^2 \phi_1}{2\varepsilon_3}, & (\Delta p_x)^2 = \cos^2 \phi_1 \frac{\varepsilon_1}{2} + \sin^2 \phi_1 \frac{\varepsilon_3}{2}, \\ (\Delta y)^2 = \frac{\cos^2 \phi_2}{2\varepsilon_2} + \frac{\sin^2 \phi_2}{2\varepsilon_3}, & (\Delta p_y)^2 = \cos^2 \phi_2 \frac{\varepsilon_2}{2} + \sin^2 \phi_2 \frac{\varepsilon_3}{2}, \\ (\Delta z)^2 = \frac{\sin^2 \phi_1}{2\varepsilon_1} + \frac{\sin^2 \phi_2}{2\varepsilon_2} + \frac{(\cos \phi_1 + \cos \phi_2)^2}{2\varepsilon_3} - \frac{1 + 2 \cos \phi_1 \cos \phi_2}{2\omega_m}, \\ (\Delta p_z)^2 = \sin^2 \phi_1 \frac{\varepsilon_1}{2} + \sin^2 \phi_2 \frac{\varepsilon_2}{2} + (\cos \phi_1 + \cos \phi_2)^2 \frac{\varepsilon_3}{2} - (1 + 2 \cos \phi_1 \cos \phi_2) \frac{\omega_m}{2}. \end{cases} \quad (75)$$

基于 (75) 式, 对应于图 4, 图 8 给出了压缩方差 $(\Delta x)^2 \omega_m$, $(\Delta y)^2 \omega_m$ 和 $(\Delta z)^2 \omega_m$ (实线), $(\Delta p_x)^2 / \omega_m$, $(\Delta p_y)^2 / \omega_m$ 和 $(\Delta p_z)^2 / \omega_m$ (虚线) 随耦合参数 G_1 / ω_m 和 G_2 / ω_m 的变化. 图 8(a) 中 $(\Delta x)^2 \omega_m$ 和 $(\Delta z)^2 \omega_m$ 重合, $(\Delta p_x)^2 / \omega_m$ 和 $(\Delta p_z)^2 / \omega_m$ 重合, 坐标方差开始

没有被压缩, 而后被渐渐压缩, 在接近临界耦合 G_{1c} 时, 被最大压缩 (如图点竖线), 如图实线; 反之, 动量方差开始被压缩, 而接近临界耦合 G_{1c} 时, 反而不被压缩, 如图虚线. 图 8(b) 中 $(\Delta y)^2 \omega_m$ 和 $(\Delta z)^2 \omega_m$ 重合, $(\Delta p_y)^2 / \omega_m$ 和 $(\Delta p_z)^2 / \omega_m$ 重合, 坐标

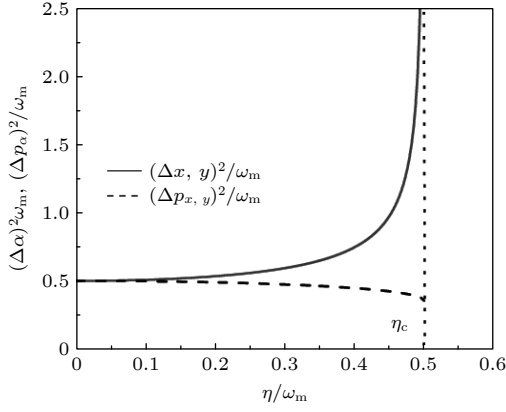


图 7 在 $\omega = \omega_m$ 下, 压缩方差 $(\Delta\alpha)^2\omega_m$ 和 $(\Delta p_\alpha)^2/\omega_m$ 随耦合参数 η/ω_m 的变化

Fig. 7. Plot of the squeezing variances $(\Delta\alpha)^2\omega_m$ (solid line) and $(\Delta p_\alpha)^2/\omega_m$ (dashed line) as a function of η/ω_m in the case of $\omega = \omega_m$.

方差开始未被压缩, 而后被渐渐压缩, 在接近临界耦合 G_{2c} 时, 被最大压缩 (如图点线), 如图实线; 反之, 动量方差开始被压缩, 而接近临界耦合 G_{2c} 时, 反而不被压缩, 如图虚线. 该结论再次验证图 4 中激发谱在动力学临界点处的相变和能量转移一致. 可见, 压缩是能量转换的标志. 在 $G_1 < G_{1c}$ ($G_2 < G_{2c}$) 时, 动量方差被压缩, 则动量正交就是更好的选择; 而在 G_{1c} (G_{2c}) 附近, 动量方差未被压缩, 而坐标方

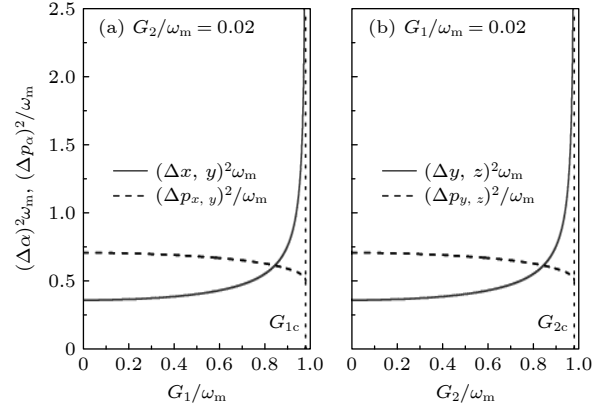


图 8 在 $(\Delta\alpha)^2\omega_m$ 下, 压缩方差 $(\Delta\alpha)^2\omega_m$ 和 $(\Delta p_\alpha)^2/\omega_m$ 随耦合参数 (a) G_1/ω_m 和 (b) G_2/ω_m 的变化

Fig. 8. Plot of the squeezing variances $(\Delta\alpha)^2\omega_m$ (solid line) and $(\Delta p_\alpha)^2/\omega_m$ (dashed line) as a function of (a) G_1/ω_m and (b) G_2/ω_m .

差被压缩, 则坐标正交将是更好的选择. 可见, 三模玻色场中的任何的正交压缩是由特定玻色模之间的能量交换决定^[19,20], 其可借助于不同的耦合参数来调控.

3.2.2 双光腔间有耦合

本节研究了光腔间有耦合的双模光机械腔的压缩特性. 原始玻色模 $[a_1, a_2, b]$ 和重新量化的玻色模 $[c_1, c_2, c_3]$ 之间的关系利用波戈留波夫变换给出:

$$a_1^\dagger = \frac{1}{2} \left\{ \frac{\cos \phi_1 + \cos \phi_2}{\sqrt{\Omega_1 \varepsilon_I \sqrt{\varepsilon_{pI}}}} \left[c_1^\dagger (\sqrt{\varepsilon_{pI}} \Omega_1 + \varepsilon_I) + c_1 (\sqrt{\varepsilon_{pI}} \Omega_1 - \varepsilon_I) \right] + \frac{\sin \phi_1}{\sqrt{\varepsilon_{pII} \Omega_1 \varepsilon_{II}}} \left[c_2^\dagger (\sqrt{\varepsilon_{pII}} \Omega_1 + \varepsilon_{II}) + c_2 (\sqrt{\varepsilon_{pII}} \Omega_1 - \varepsilon_{II}) \right] + \frac{\sin \phi_2}{\sqrt{\Omega_1 \varepsilon_{III}}} \left[c_3^\dagger (\Omega_2 + \varepsilon_{III}) + c_3 (\Omega_2 - \varepsilon_{III}) \right] \right\}, \quad (76)$$

$$a_2^\dagger = \frac{1}{2} \left\{ \frac{-\sin \phi_1}{\sqrt{\Omega_2 \varepsilon_I \sqrt{\varepsilon_{pI}}}} \left[c_1^\dagger (\sqrt{\varepsilon_{pI}} \Omega_2 + \varepsilon_I) + c_1 (\sqrt{\varepsilon_{pI}} \Omega_2 - \varepsilon_I) \right] + \frac{\cos \phi_1 + \cos \phi_3}{\sqrt{\varepsilon_{pII} \Omega_2 \varepsilon_{II}}} \left[c_2^\dagger (\sqrt{\varepsilon_{pII}} \Omega_2 + \varepsilon_{II}) + c_2 (\sqrt{\varepsilon_{pII}} \Omega_2 - \varepsilon_{II}) \right] + \frac{\sin \phi_3}{\sqrt{\Omega_1 \varepsilon_{III}}} \left[c_3^\dagger (\Omega_2 + \varepsilon_{III}) + c_3 (\Omega_2 - \varepsilon_{III}) \right] \right\}, \quad (77)$$

$$b^\dagger = \frac{1}{2} \left\{ \frac{-\sin \phi_2}{\sqrt{\omega_m \varepsilon_I \sqrt{\varepsilon_{pI}}}} \left[c_1^\dagger (\sqrt{\varepsilon_{pI}} \omega_m + \varepsilon_I) + c_1 (\sqrt{\varepsilon_{pI}} \omega_m - \varepsilon_I) \right] + \frac{\sin \phi_3}{\sqrt{\omega_m \varepsilon_{II} \sqrt{\varepsilon_{pII}}}} \left[c_2^\dagger (\sqrt{\varepsilon_{pII}} \omega_m + \varepsilon_{II}) + c_2 (\sqrt{\varepsilon_{pII}} \omega_m - \varepsilon_{II}) \right] + \frac{\cos \phi_2 + \cos \phi_3}{\sqrt{\omega_m \varepsilon_{III}}} \left[c_3^\dagger (\omega_m + \varepsilon_{III}) + c_3 (\omega_m - \varepsilon_{III}) \right] \right\}. \quad (78)$$

基于 (76) 式—(78) 式, 各变量的方差被给出:

$$\left\{ \begin{array}{l} (\Delta x)^2 = \frac{(\cos \phi_1 + \cos \phi_2)^2 \sqrt{\varepsilon_{p_I}}}{2\varepsilon_I} + \frac{\sin^2 \phi_1 \sqrt{\varepsilon_{p_{II}}}}{2\varepsilon_{II}} + \frac{\sin^2 \phi_2}{2\varepsilon_{III}} - \frac{1 + 2 \cos \phi_1 \cos \phi_2}{2\Omega_1}, \\ (\Delta p_x)^2 = (\cos \phi_1 + \cos \phi_2)^2 \frac{\varepsilon_I}{2\sqrt{\varepsilon_{p_I}}} + \sin^2 \phi_1 \frac{\varepsilon_{II}}{2\sqrt{\varepsilon_{p_{II}}}} + \sin^2 \phi_2 \frac{\varepsilon_{III}}{2} - (1 + 2 \cos \phi_1 \cos \phi_2) \frac{\Omega_1}{2}, \\ (\Delta y)^2 = \frac{\sin^2 \phi_1 \sqrt{\varepsilon_{p_I}}}{2\varepsilon_I} + \frac{(\cos \phi_1 + \cos \phi_3)^2 \sqrt{\varepsilon_{p_{II}}}}{2\varepsilon_{II}} + \frac{\sin^2 \phi_3}{2\varepsilon_{III}} - \frac{1 + 2 \cos \phi_1 \cos \phi_3}{2\Omega_2}, \\ (\Delta p_y)^2 = \sin^2 \phi_1 \frac{\varepsilon_I}{2\sqrt{\varepsilon_{p_I}}} + (\cos \phi_1 + \cos \phi_3)^2 \frac{\varepsilon_{II}}{2\sqrt{\varepsilon_{p_{II}}}} + \sin^2 \phi_3 \frac{\varepsilon_{III}}{2} - (1 + 2 \cos \phi_1 \cos \phi_3) \frac{\Omega_2}{2}, \\ (\Delta z)^2 = \frac{\sin^2 \phi_2 \sqrt{\varepsilon_{p_I}}}{2\varepsilon_I} + \frac{\sin^2 \phi_3 \sqrt{\varepsilon_{p_{II}}}}{2\varepsilon_{II}} + \frac{(\cos \phi_2 + \cos \phi_3)^2}{2\varepsilon_{III}} - \frac{1 + 2 \cos \phi_2 \cos \phi_3}{2\omega_m}, \\ (\Delta p_z)^2 = \sin^2 \phi_2 \frac{\varepsilon_I}{2\sqrt{\varepsilon_{p_I}}} + \sin^2 \phi_3 \frac{\varepsilon_{II}}{2\sqrt{\varepsilon_{p_{II}}}} + (\cos \phi_2 + \cos \phi_3)^2 \frac{\varepsilon_{III}}{2} - (1 + 2 \cos \phi_2 \cos \phi_3) \frac{\omega_m}{2}. \end{array} \right. \quad (79)$$

基于 (79) 式, 对应于图 6, 图 9 给出了压缩方差 $(\Delta x)^2 \omega_m$, $(\Delta y)^2 \omega_m$ 和 $(\Delta z)^2 \omega_m$ (实线), $(\Delta p_x)^2 / \omega_m$, $(\Delta p_y)^2 / \omega_m$ 和 $(\Delta p_z)^2 / \omega_m$ (虚线) 随耦合参数 δ / ω_m , J_1 / ω_m 和 J_2 / ω_m 的变化. 图 9(a) 结果与图 7 一致, 如图所示, 坐标方差没有被压缩, 在接近临界耦合 δ_c 时, 更加不被压缩而分离, 如图实线; 动量方差被压缩, 而且接近临界耦合 η_c 时, 压缩更明显, 动力学临界点处动量方差显示最大压缩, 如图虚线. 相比之下, 图 9(b) 和图 9(c) 结果与图 8 一致. 图 9(b) 和图 9(c) 表明: 随着耦合参数 J_1 (J_2) 的增加, 最初未被压缩的动量方差慢慢被稍微受到压缩. 在临界耦合 J_{1c} (J_{2c}) 附近, 动量方差接近 $1/2$, 并在 J_{1c} (J_{2c}) 处被最大压缩. 而最初被压缩的坐标方差随耦合强度增大而慢慢变小, 并且在 J_{1c} (J_{2c}) 处变得不被压缩. 事实上, 随着位置方差的不确定性降低,

而相应动量方差的不确定性增加, 这与不确定性原理一致. 因此得出结论, 正交压缩是最适合量子测量, 因为正交压缩减少了量子噪声, 即如果在改变 δ 时进行量子测量, 那么对坐标正交进行测量会更合适. 另一方面, 在改变耦合参数 J_1 (J_2) 时, 只要被挤压, 坐标正交就是更好的选择. 在临界点 J_{1c} (J_{2c}) 附近, 动量正交的测量将更适合. 在三模玻色场中的任何正交压缩是由特定玻色模之间的能量交换决定^[19,20], 其可以借助于不同的耦合参数来调控. 如图 6 所示, 任何两模之间的能量转换在动力学临界点处完成. 图 9 展示出于动力学临界点, 坐标正交或动量正交显示最大压缩. 因此, 压缩是能量转移的标志 (即压缩由多模间的能量转换度决定).

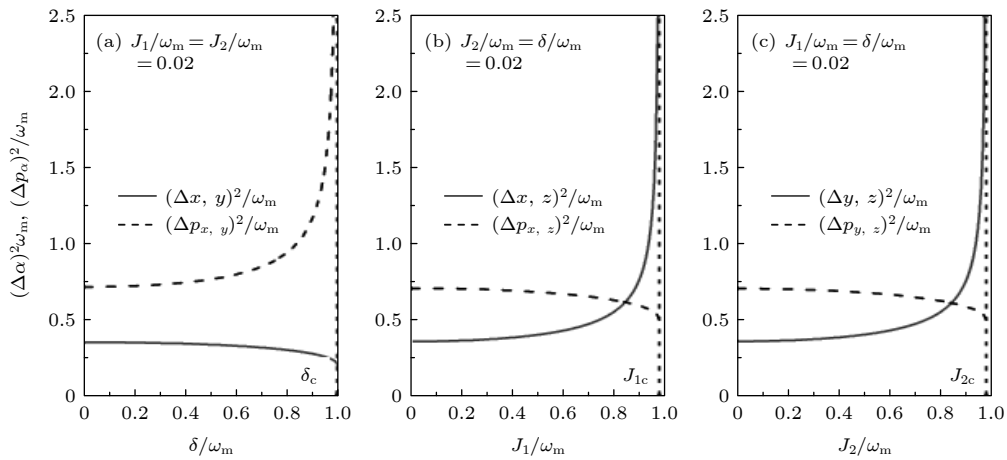


图 9 在 $\omega = \omega_m$ 下, 压缩方差 $(\Delta \alpha)^2 \omega_m$ (实线) 和 $(\Delta p_\alpha)^2 / \omega_m$ (虚线) 随耦合参数 (a) δ / ω_m , (b) J_1 / ω_m 和 (c) J_2 / ω_m 的变化
Fig. 9. Plot of the squeezing variances $(\Delta \alpha)^2 \omega_m$ (solid line) and $(\Delta p_\alpha)^2 / \omega_m$ (dashed line) as a function of (a) δ / ω_m , (b) J_1 / ω_m , (c) J_2 / ω_m in the case of $\omega = \omega_m$.

4 结 论

本文首先利用动力学方法分别对单模光机械系统和双模光机械系统进行了哈密顿量的线性, 进而求得了系统的稳态解. 基于稳态解给出了不同参数调控下的激发谱和模压缩, 探究了光机械系统中的动力学相变与光学模和机械模之间能量选择性转换的可能性. 尤其单模光机械系统清晰地给出了光学模和机械模之间的能量转换, 为理解双模光机械系统的动力学相变和能量交换提供了指导. 另外, 激发谱和模压缩之间的关联也被观测. 通过调节某一模对应的耦合参数, 可以对应地打开该模通道, 而进行其他模之间的能量交换, 且同时也关闭了其他模的通道. 该通道和其他模式间的能量交换都是可选择的, 这对于量子信息处理是非常有实际意义的. 在动力学临界点处, 任何两模之间完全的能量转换可实现. 通过坐标和动量方差的研究发现: 被压缩的正交变量最适合进行测量, 因为量子噪声量较小. 另外, 声子模可以较长时存储能量, 而光子模可以远距离传输能量, 这种优势使得混合光机械系统在将来产生量子通信和量子信息处理单元中变得非常有价值.

参考文献

- [1] Marquardt F, Girvin S M 2009 *Physics* **2** 40
- [2] Brennecke F, Ritter S, Donner T, Esslinger T 2008 *Science* **322** 235
- [3] Safavi-Naeini A H, Mayer Alegre T P, Chan J, Eichenfield M, Winger M, Lin Q, Hill J T, Chang D E, Painter O 2011 *Nature* **478** 89
- [4] Verhagen E, Deléglise S, Weis S, Schliesser A, Kippenberg T J 2012 *Nature* **482** 63
- [5] Kumar T, Bhattacharjee A, ManMohan 2010 *Physical Review A* **81** 013835
- [6] Thompson J D, Zwickl B M, Jayich A M, Marquardt F, Girvin S M, Harris J G E 2008 *Nature* **452** 900
- [7] Antonio D, Czaplewski D A, Guest J R, López D 2015 *Phys. Rev. Lett.* **114** 034103
- [8] Stannigel K, Komar P, Habraken S J M, Bennett S D, Lukin P, Zoller P, Rabl P 2012 *Phys. Rev. Lett.* **109** 013603
- [9] Chang D E, Safavi-Naeini A H, Hafezi M, Painter O 2011 *New Journal of Physics* **13** 023003
- [10] Emary C, Brandes T 2003 *Phys. Rev. E* **67** 066203
- [11] Liu N, Wang J F, Liang J Q 2020 *Acta Phys. Sin.* **69** 064202 (in Chinese) [刘妮, 王建芬, 梁九卿 2020 物理学报 **69** 064202]
- [12] Zhao X Q, Liu N, Bai X M, Liang J Q 2017 *Ann. Phys.* **378** 448
- [13] Xuereb A, Barbieri M, Paternostro M 2012 *Physical Review A* **86** 013809
- [14] Xu K, Sun Z, Liu W, Zhang Y, Li H, Dong H, Ren W, Zhang P, Nori F, Zheng D, Fan H, Wang H 2020 *Science Advances* **6** eaba4935
- [15] Yan B, Chernyak V Y, Zurek W H, Sinitsyn N A 2021 *Phys. Rev. Lett.* **126** 070602
- [16] Leroze A, Marino J, Zunkovic B, Gambassi A, Silva A 2018 *Phys. Rev. Lett.* **120** 130603
- [17] Nicola S, Michailidis A, Serbyn M 2021 *Phys. Rev. Lett.* **126** 040602
- [18] Korolkova N, Perina J 1997 *Optics Communications* **136** 135
- [19] Korolkova N, Perina J 1997 *Journal of Modern Optics* **44** 1525
- [20] Gröblacher S, Hammerer K, Vanner M R, Aspelmeyer M 2009 *Nature* **460** 724

Dynamical phase transition and selective energy exchange in dual-cavity optomechanical systems^{*}

Liu Ni[†] Zhang Xiao-Fang Liang Jiu-Qing

(*State Key Laboratory of Quantum Optics and Quantum Optics Devices, Institute of Theoretical Physics, Shanxi University, Taiyuan 030006, China*)

(Received 25 January 2021; revised manuscript received 2 March 2021)

Abstract

In recent years, the cavity quantum photomechanics has been developed rapidly, and played a very important role in quantum information processing, quantum basic principle verification, and high-precision measurement. The kinds of quantum mechanical behaviors have also been explored and discovered in the study of cavity mechanics. By placing the Kerr medium in the system, quantum nonlinearity is introduced into the optomechanical system. Quantum phase transition is a relatively important part in the research of condensed matter physics. Since Dicke quantum phase transition was successfully observed experimentally, the problem of quantum phase transition in the optical cavity has attracted more attention. The spin-coherent-state variation method and the Holstein-Primakoff transformation are used to theoretically calculate the ground state energy functional, and the rich structure of the macroscopic multi-particle quantum state is given by adjusting the parameters. The quantum phase transition evolution equation describes the relationship between each phase and the time of generating a new phase when reaching the critical phase transition point. At the same time, the mode squeezing of multi-mode hybrid optomechanical system has also become one of the basic problems of quantum mechanical behavior in cavity quantum dynamics.

In this article, we explore the quantum dynamics of optomechanical devices including single-cavity and dual-cavities. We find that the system will undergo a dynamic phase transition, which is similar to the Dicke-Hepp-Lieb superradiant type phase transition, and a new dynamic critical point appears in the coupling between the momentum quadratures of the two optical fields. By manipulating the coupling parameters, we can achieve selective energy exchange between any two modes and the critical coupling point corresponds to selective energy exchange. Mode squeezing, which is easy to measure by applying the quantum uncertainty relationship, is also revealed and consistent with selective energy exchange. The study of coordinate and momentum variances gives us the revelation that the compressed orthogonal variables are the most suitable for measurement because of the small quantum noise. In fact, phononic modes can store energy in a longer duration, while photonic modes can transfer energy in a long distance. This phenomenon makes the hybrid optomechanical cavities useful in the next-generation quantum communications and quantum information processing units.

Keywords: dual-cavities optomechanical system, phase transition, selective energy exchange, mode squeezing

PACS: 03.65.-w, 42.50.Pq, 05.30.Rt, 73.43.Nq

DOI: 10.7498/aps.70.20210178

^{*} Project supported by the National Natural Science Foundation of China (Grant Nos. 11772177, 12047571) and the Scientific and Technological Innovation Programs of Higher Education Institutions in Shanxi Province (STIP), China (Grant No. 2019L0069).

[†] Corresponding author. E-mail: 317446484@qq.com